PAPER

Check for updates

Innovative wound management: creating dynamic Alg-Mg/SF hydrogels for controlled Mg²⁺ release in wound healing†

Chaolun Dai,‡[ab] Binxin Wu,‡[c] Min Chen,[b] Yisheng Gao,[a] Miao Zhang,[a] Wanhua Li,[a] Guicai Li,[a] Qinzhi Xiao,*[bd] Yahong Zhao*[a] and Yumin Yang [iD] *[a]

Antibacterial hydrogels have gained considerable attention for soft tissue repair, particularly in preventing infections associated with wound healing. However, developing an antibacterial hydrogel that simultaneously possesses excellent cell affinity and controlled release of metal ions remains challenging. This study introduces an antibacterial hydrogel based on alginate modified with bisphosphonate, forming a coordination complex with magnesium ions. The hydrogel, through an interpenetrating network with silk fibroin, effectively controls the release of magnesium ions and enhances strain resistance. The Alg-Mg/SF hydrogel not only demonstrates outstanding biocompatibility and broad-spectrum antibacterial properties but also stimulates macrophages to secrete anti-inflammatory factors. This advanced Alg-Mg/SF hydrogel provides a convenient therapeutic approach for chronic wound management, showcasing its potential applications in wound healing and other relevant biomedical fields.

Introduction

Among various pathogenic agents, bacterial infection of biological scaffolds and implanted devices, such as artificial grafts, catheters, endotracheal tubes, and prosthetic joints, poses a serious public health problem.[1–3] Infection with pathogenic microorganisms can greatly reduce wound healing and tissue repair,[4] even to the point of non-healing and non-repair.[5] In addition, the misuse and overuse of common antibiotics have accelerated the spread of drug-resistant bacteria, which makes it difficult to control a variety of infectious diseases.[6] Therefore, there is an urgent need for a solution to the problem of antimicrobial resistance.[7] The development of multifunctional and easily-synthesized effective antibacterial scaffolds has bloomed.[8]

Alternative antimicrobial agents with unique bioactivities, excellent biocompatibility and more efficient antimicrobial performance against a broad range of pathogens would be

[a]Key Laboratory of Neuroregeneration of Jiangsu and Ministry of Education, Co-innovation Center of Neuroregeneration, NMPA Key Laboratory for Research and Evaluation of Tissue Engineering Technology Products, Nantong University, Nantong 226001, P. R. China

[b]Medical School, Nantong University, Nantong 226001, P. R. China

[c]Department of Echocardiography Centre, Affiliated Hospital of Nantong University, 226001, Nantong, P. R. China

[d]Department of Pediatrics, Affiliated Hospital of Nantong University, 226001, Nantong, P. R. China

† Electronic supplementary information (ESI) available. See DOI: https://doi.org/10.1039/d4ra00793j

‡ The authors contributed equally to this work.

greatly preferable in this aspect.[9] Nowadays, hydrogels have a wide range of applications from biological scaffolds to medical devices due to their distinguished merits, including environmental friendliness, resource regeneration, low cost, *etc.*[10,11] Currently, the most crucial factors in designing antibacterial hydrogel wound dressings are the selection of raw materials and crosslinking methods.[12] Generally, commonly used raw materials for hydrogels include natural, synthetic, and semi-synthetic materials. Based on raw materials, antibacterial substances, and antibacterial mechanisms, antibacterial hydrogel wound dressings can be classified into three categories: (i) intrinsic antibacterial hydrogel wound dressings; (ii) antimicrobial agent-releasing hydrogel wound dressings; (iii) environmentally responsive antibacterial hydrogel wound dressings. Hydrogels with different crosslinking networks can be categorized into (i) dynamic physically crosslinked hydrogels, including electrostatic interactions, hydrogen bonds, crystallization, host–guest interactions, and cation-π interactions; (ii) chemically crosslinked hydrogels, relying on robust covalent bonds to construct the three-dimensional network of the hydrogel; (iii) hydrogels with mixed networks, where physical and covalent bonds cooperate to build the hydrogel network.[13] Structurally dynamic hydrogels emulate the dynamic structural properties of natural extracellular matrix (ECM) and can better mimic the dynamics and functions of ECM, thereby enhancing the effect of biofunctionalization.[14] The dynamic hydrogels can sense and respond to localized physicochemical forces and biological signals, which possess inherent bioactivities that mediate the desired behaviors of the cells. Natural polymers are among the convenient additives for hydrogels

because they meet many of these criteria such as antimicrobial, antiviral, and antifungal features.[15]

Silk fibroin (SF), a fibrous protein derived from the cocoons of domestic silkworm *Bombyx mori*, exhibits low immunogenicity, remarkable biocompatibility and unique mechanical properties, thus emerging as a promising biomaterial. Despite SF is lack of inherent antibacterial activity, different processing procedures and chemical modifications have been devoted to confer SF scaffolds with antibacterial properties. The many outstanding properties of SF that qualify it for a wide range of applications in combination with other biomaterials.

Alginate is a naturally-occurring, linear anionic polysaccharides consisting of β-D-mannuronate (M-blocks) and α-L-guluronate (G-blocks) residues linked by β-glycosidic bonds.[16] The units can be arranged in either blocks or segments of various lengths in a MM, MG and GG pattern depending on the extraction procedure.[17–19] Molecule structure of the alginate allows electrostatic interactions and a high degree of coordination with ions, resulting in the construction of ionically cross-linked dynamic hydrogels for various biomedical applications.[20] Several studies have demonstrated the potential application of alginate hydrogel in antibacterial scaffolds, which was attributed to the effects of alginate on weakening the pathogenic biofilm structures.[18,21] The physicochemical, antimicrobial, and antioxidant properties of alginate hydrogels can be extended by incorporating synthetic or natural active compounds.[20]

Inorganic metal ions (Ag, Zn, Au, Cu, Mg) and their metal oxide nanoparticles exhibit broad-spectrum antibacterial properties.[22] Silver, with its long history as an antibacterial material, possesses excellent bactericidal capabilities. However, the effective concentration range and safe concentration range for antibacterial action of silver ions are relatively narrow, and excessively high concentrations may pose toxicity to human cells. Magnesium (Mg) and its alloys exhibit good biocompatibility, anti-bacterial effect, anti-inflammation and anti-tumor function properties.[23] Recent attempts using Mg alloys as potential biomaterials and promising alternatives for medical implants have demonstrated their ability in biomedical applications.[24] Mg ions (Mg^{2+}) are formed upon Mg degradation are one of the most important cofactors of many enzymes. The oral administration of Mg^{2+} has been reported to correlate with the magnesium transporter genes, regulate inflammatory response and promote peripheral nerve regeneration. Moreover, the application of Mg after traumatic brain injury or stroke improves functional recovery. Mg^{2+} is reported to not only regulate cellular behaviors but can also act directly on bacteria, affecting the membranes of the bacterial cells.[25] Mg metal filaments placed inside a nerve guide conduit have been reported to improve the rate and extent of regeneration across a short nerve injury gap. However, they showed unsatisfactory effects for the larger nerve defects due to fast degradation of magnesium resulting in the local accumulation of Mg^{2+} ions. Therefore, the development of biomaterial vehicles systems are required for controlled delivery of Mg^{2+} release. In our previous research, we successfully achieved controlled release of magnesium ions to avoid excessive accumulation while promoting nerve regeneration.[26] Considering the outstanding

biological effects of magnesium ions, it is essential to develop a hydrogel capable of sustained release of magnesium ions for application in the field of wound healing.

In this study, we developed a novel adaptable hydrogel. Owing to highly dynamic interactions between bisphosphonate-modified alginate (Alg-BP) and Mg^{2+}, the obtained hydrogels exhibited remarkable dynamic properties, and the thiol–ene click reaction between glutathione (GSH) and methacryloyl (MA) groups on SF created the interpenetrating polymer network (IPN). This IPN hydrogel, while enhancing the mechanical properties of physically cross-linked hydrogels, achieves prolonged broad-spectrum antibacterial capability through controlled release of magnesium ions. Due to its simple preparation and excellent biocompatibility of individual components, Alg-Mg/SF not only exhibits outstanding antibacterial performance but also maintains excellent biocompatibility. Additionally, the presence of magnesium ions stimulates M1 macrophages to secrete more anti-inflammatory factors, thus counteracting inflammatory responses. In short, this study proposes a contact-active antibacterial hydrogel with an efficient bactericidal mechanism, which may play a crucial role in accelerating soft tissue repair and protecting wounds from bacterial infections.

Materials and methods

Synthesis of bisphosphonated-alginate (Alg-BP)

The bisphosphonated-alginate (Alg-BP) was synthesised as described previously26. Briefly, pamidronate disodium was dissolved in MES buffer. Then, Alg (Mingyue, Chian) was added into the above solution, followed by the addition of *N*-hydroxysuccinimide (NHS, Sigma, USA) and 1-(3-dimethylaminopropyl)-3-ethylcarbodiimide hydrochloride (EDC, Sigma, USA) in turn. The reaction was proceeded for 24 hours at room temperature, followed by dialyze against NaCl gradient solution for 3 days, frozen at -80 °C temperature, lyophilized and stored at 20 °C powder form.

Preparation of silk fibroin stock solution

Then, glutathione (GSH, Sigma, USA) was added to a final concentration of 2 g l^{-1} into the above mixture. The reaction is carried out for 1 h at room temperature, and the unreacted GSH in the solution were removed by dialysis. To gain the highly concentrated SF-GSH solution, the aqueous SF-GSH solution was subjected to airflow at 4 °C to evaporate the water and prevent the SF-GSH from self-crosslinking. The SF methacryloyl (SF-MA) was purchased from Yongqinquan (China) and dissolved in DI water at 10 mg ml^{-1}.

Preparation of the Alg/SF hydrogels

Alg-BP was dissolved in HEPES buffer (pH = 7.4), followed by mixing with the concentrated solution of SF-GSH and SF-MA. The hydrogels were cast by rapidly mixing the Alg-BP/SF solution with a CaSO4 or $MgCl_2$ slurry *via* two syringes and ejecting the mixture between two glass plates, where it gelled over 0.5 h. Four different hydrogels were designed, *i.e.*, Alg hydrogel, Alg-

Mg hydrogel, Alg/SF hydrogel, and Alg-Mg/SF hydrogel, respectively (Table S1†).

SEM characterization

The microscopic morphology of the cross-section of the hydrogel was observed by scanning electron microscopy. After being frozen by liquid nitrogen and lyophilized, the hydrogel specimens were cut in half, fixed on a stage, and sprayed with a thin layer of gold. Images were acquired at an accelerating voltage of 30 kV, and at least 50 pores in each sample were measured randomly to analyze the pore size of the hydrogels.

Mechanical properties

The compressive mechanical properties of the Alg/SF IPN hydrogels were tested with an electronic universal testing machine (C43.104Y, MTS SYSTEMS Co. Ltd). The Cylindrical Alg/SF IPN hydrogels with 2 mm length and 10 mm diameter were placed on the pedestal and the universal testing machine was set in compression mode. After that, the data were zeroed and compressed at 2 mm min^{-1} with loading force of 50 N, and the data was continuously recorded until a deformation rate of 50% was achieved. All tests were carried out in ambient environment (25 °C temperature, $\approx$45% humidity) with three repeat specimens. After the test, the stress–strain curve was obtained. The elasticity modulus of the samples was obtained by calculating the slope of the stress–strain curve.

Hydrophilicity test

The hydrophilicity of the hydrogel samples was evaluated using contact angle measurements. Prior to analysis, any excess surface water was carefully removed from the hydrogel. The samples were then precisely positioned on a level measurement platform. A meticulously controlled, single drop of distilled water was gently deposited onto the surface of each hydrogel sample. The angle of contact formed between the water droplet and the hydrogel surface was then accurately measured. This process was repeated for a minimum of three independent measurements per sample, ensuring the reliability and reproducibility of the results.

Quantification of the release of magnesium ions from hydrogels

The Alg-Mg or Alg-Mg/SF hydrogels were immersed in HEPES buffer (pH = 7.4, containing 2 mM Ca^{2+}) under 37 °C. 100 μl of supernatant was collected at each preset time point followed by the addition of 100 μl of fresh buffer or solution. All samples were in triplicate ($n = 3$). The supernatant samples were analyzed by magnesium colorimetric assay kit (Nanjing Jiancheng) according to manufacturer's protocol.

Cell viability

L929 was cultivated in Dulbecco's modified Eagle's medium (DMEM) supplemented with 10% fetal bovine serum (FBS) at 37 °C in a 5% CO$_2$. The Alg/SF IPN hydrogels were extracted with the above DMEM medium at a volume ratio of 1 : 10 for 24 h.

After being planted into a 96-well plate with a density of 5000 per well, L929 cells were cultured in hydrogel extracts culture medium (100 μl) and normal medium as controls. After incubation for 1 and 3 d, the culture medium in the well plates was discarded, and 200 μl of Cell Counting Kit-8 (CCK-8) solution was added to the experimental wells and blank wells and incubated for another 4 h. Then, the absorbance of culture medium was measured by a microplate reader (Bio-Tek, Winooski, VT, USA) at 450 nm. In each group, five independent samples were investigated and then averaged.

Trypan blue test

L929 cell line was detached from the hydrogel matrix using a pancreatic enzyme solution. The cell suspension was then subjected to centrifugation at 1000 rpm for 5 minutes to facilitate cell sedimentation. The cell pellet was resuspended in 1 ml of culture medium using a micropipette to obtain a homogeneous single-cell suspension. An aliquot of 100 μl was extracted from the suspension to create equal test samples. To these, 100 μl of a 0.4% Trypan Blue (TB) solution was added, achieving a final dilution of 1 : 2. The mixture was allowed to incubate for 5 minutes, enabling the Trypan Blue to stain dead cells. Following the incubation, cell viability was assessed by counting the stained (non-viable) and unstained (viable) cells using a hemocytometer and optical microscope.

In vitro antibacterial activity

The hydrogels were soaked and washed with sterilized ddH$_2$O for 24 hours to remove bacteria. *S. aureus* and *E. coli* were used to evaluate the antibacterial activity of the hydrogels. The bacterial suspension (10 μl) in sterilized PBS (106 CFU ml^{-1}) was spread onto each hydrogel surface in the 24-well culture plate and incubated for 3 h and 6 h at 37 °C. And the specimens without hydrogel were set as blank group. Following incubation, all surviving bacteria in each well were resuspended with 1 ml sterilized PBS and incubated for 24 h at 37 °C. The CFU was determined in the Petri dish. Tests were repeated three times for each group.

Hemolysis assay

The hemocompatibility of Alg/SF IPN hydrogel was characterized by using a spectrophotometer. The New Zealand white rabbits were approved by the Laboratory Animal Center of Nantong University and complied with institutional and international guidelines (Approval ID: SYXK [SU] 2017-0046). Firstly, the red blood cells were collected from the central artery of New Zealand white rabbit ears. Then, EDTA was added to the collected blood cells to prevent blood coagulation, and they were purified by centrifugation at 1500 rpm min^{-1}. Next, the purified red blood cells were dispersed in cold PBS and incubated with Alg/SF IPN hydrogels in PBS at 37 °C for one hour. After incubation, the incubated samples were centrifuged at 1500 rpm min^{-1} for 5 min. 100 μl of the supernatant fluid was transferred into a 96-well culture plate and measured at 545 nm in a Bio-Rad microplate reader ($n = 5$). The morphology of red blood cells was observed by optical microscopy. Water and

saline were served as the positive control and negative control groups, respectively. The absorbance of the resulting supernatant was then measured at a wavelength of 540 nm. The rate of hemolysis was calculated using the formula:

$$\text{Hemolysis rate (\%)} = (A_s - A_n)/(A_p - A_n) \times 100\%$$

where 'A_s' represents the absorbance of the sample, 'A_n' is the absorbance of the negative control, and 'A_p' is the absorbance of the positive control.

ELISA

The RAW 264.7 cells were cocultured with Alg/SF IPN hydrogels at the density of 50 000 ml^{-1} in 24-well plates and cultured for different times. Subsequently, the cell culture medium was collected after culturing for 3 days. Tumor necrosis factor alpha (TNF-α), interleukin-4 (IL-4), interleukin-6 (IL-6) and inter- leukin- 10 (IL-10) in the culture medium were extracted and quantified according to the instructions of the TNF-α, IL-4, IL-6 and IL-10 ELISA kit (Multiscience). The absorbance at 450 nm was measured using a microplate reader and then the cytokine release level was calculated based on the OD value.

Statistical analysis

All data are presented as the means ± standard deviations (SDs).

Statistical differences were determined by performing a one-way factorial analysis of variance and Tukey's post hoc test. GraphPad Prism 8 (GraphPad Software) was used for statistical analysis. Tests were conducted with a 95% confidence interval ($\alpha < 0.05$), and statistical significance was set at $p < 0.05$.

Results

Fabrication of hydrogels and characterization

We designed the hydrogel dressings by optimizing the stock solutions of Alg-BP, SF-GSH, SF-MA, and Ca^{2+}/Mg^{2+}, resulting in the formation of the hydrogel network. Briefly, the electrostatic interaction and dynamic coordination between Alg-BP and cations led to the swift formation of the primary hydrogel
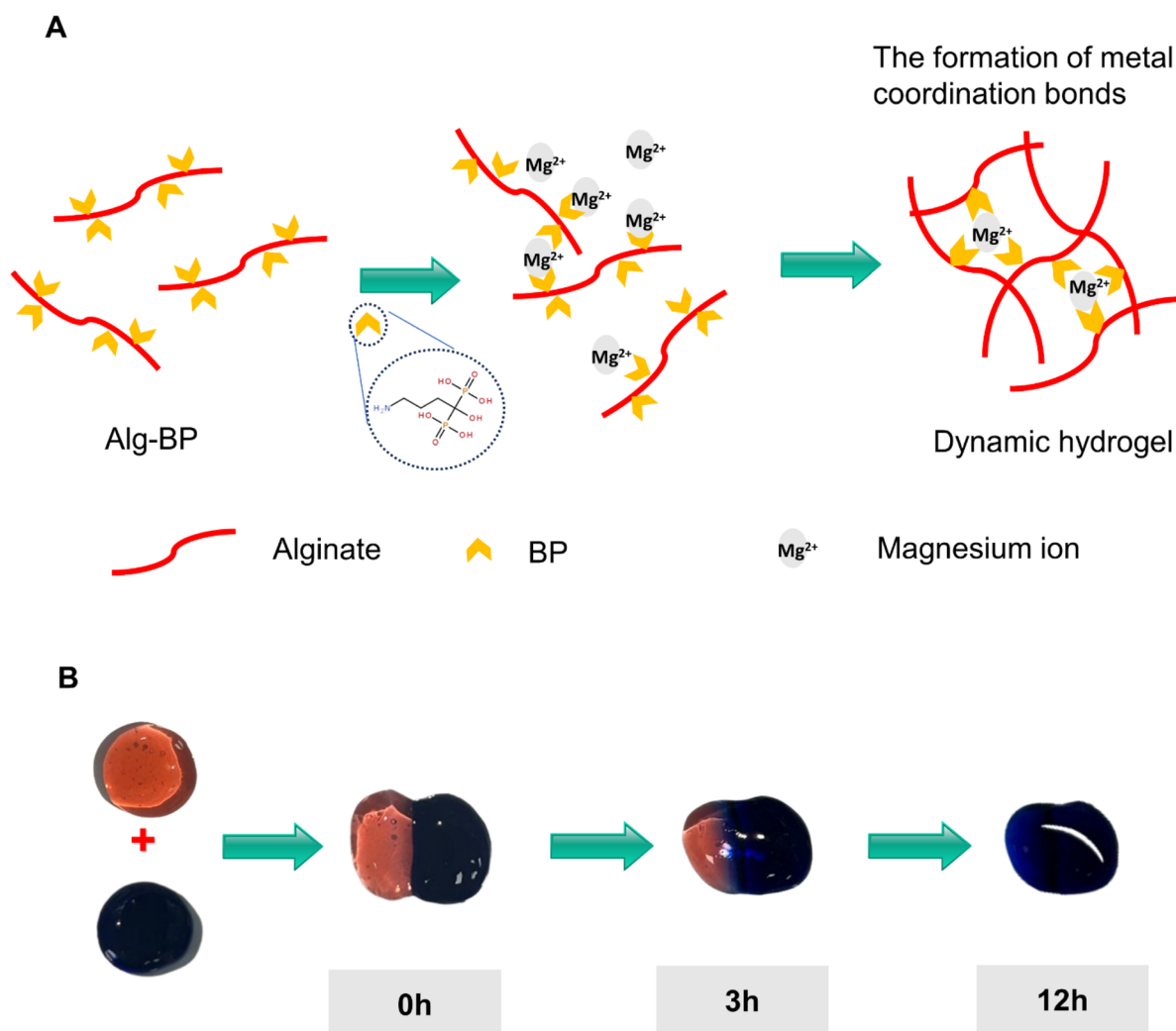

Fig. 1 Schematic illustration of the fabrication and morphological diagram of self-assembled Alg-BP-Mg^{2+} nanocomposite hydrogels. (A) The gelation mechanism of Alg-BP-Mg^{2+}. (B) Demonstrations of dynamic properties of the Alg-BP-Mg^{2+} nanocomposite hydrogels.

network, while the thiol–ene click reaction between GSH and MA groups on SF created the interpenetrating polymer network (IPN). Due to the dynamic nature of the metal coordination bonds between BP and magnesium ions (Fig. 1A), Alg-BP-Mg hydrogels can facilitate efficient ion diffusion within the 3D hydrogel network (Fig. 1B).

The observation of hydrogels using scanning electron microscopy (SEM) revealed that the pore size of Alg/SF and Alg-Mg/SF-IPN hydrogels is significantly smaller than that of Alg and Alg-Mg hydrogels (Fig. 2B and C).

Subsequently, contact angle measurements were utilized to assess the hydrophilicity of the hydrogels. The results indicated that all the hydrogel samples had relatively low contact angles. Notably, the contact angle for Alg-Mg was higher, at approximately 17° surpassing the other three groups. The Alg, Alg-Mg/SF, and Alg/SF hydrogels showed lower contact angles, around 10° or below, reflective of their greater hydrophilicity (Fig. 2B and D).

Furthermore, we assessed the incorporation of Mg^{2+} in Alg-Mg hydrogels and Alg-Mg/SF-IPN hydrogels. The results indicate that in the two-week release study, the presence of SF
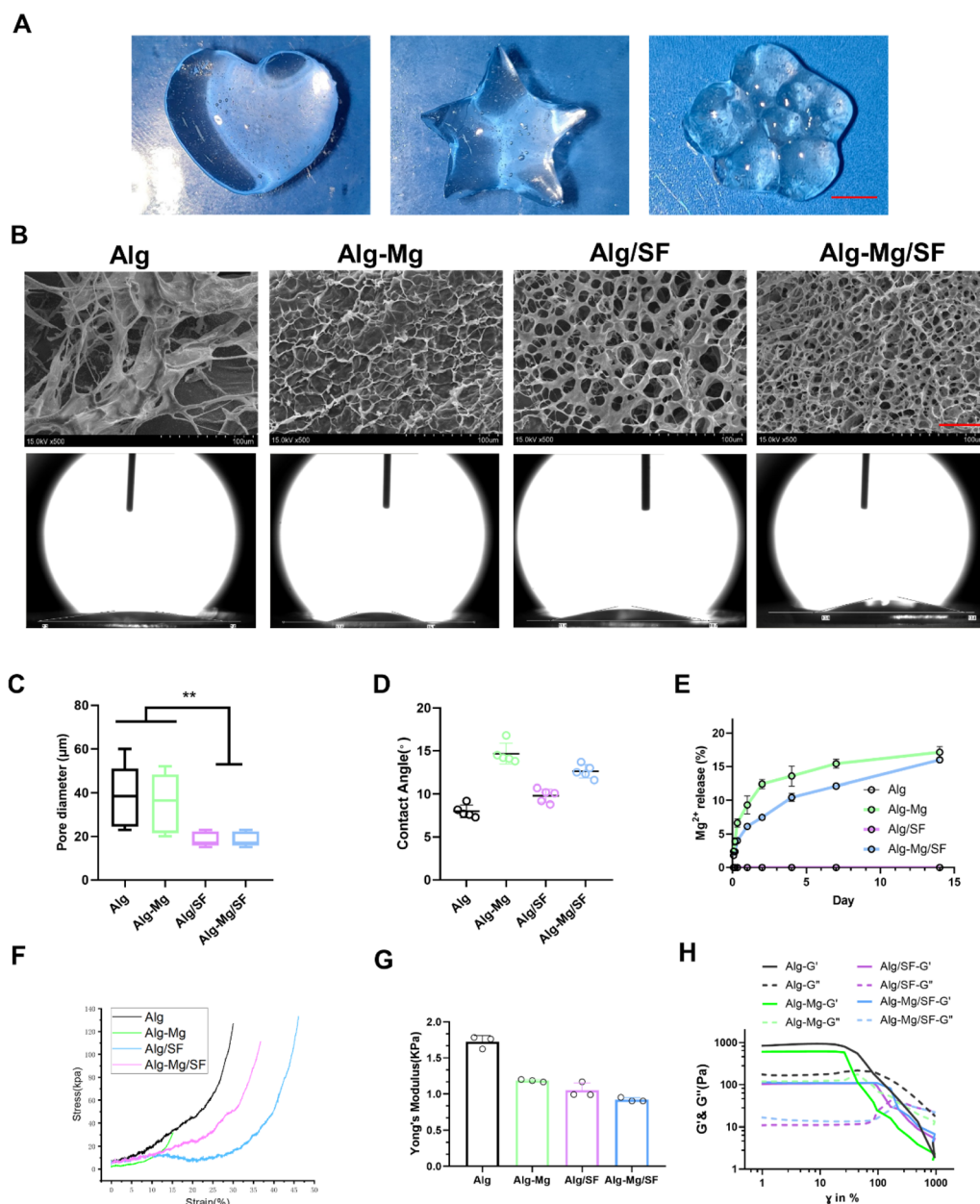

Fig. 2 Fabrication and characterization of the cell-adaptable Alg-Mg/SF hydrogel. (A) The plasticity of Alg-Mg/SF hydrogel; scale bar = 5 mm. (B) SEM characterization and photographs of water contact angles of the Alg-Mg/SF hydrogel; scale bar = 50 μm. (C) Pore size analysis of the Alg-Mg/SF hydrogel ($n = 6$). (D) Water contact angles of the Alg-Mg/SF hydrogel ($n = 5$). (E) Cumulative release profile of Mg^{2+} from the Alg-Mg/SF hydrogel in PBS over 14 days ($n = 5$); **$p < 0.01$. (F) The stress–strain curves of different hydrogel groups. (G) The Young's modulus of hydrogels from each group was determined through compression testing ($n = 3$). (H) Strain sweep from 0.01% to the crossover point of G' and G'' at a constant shear frequency of 1 Hz.

further slowed down the release of Mg^{2+} in Alg-Mg/SF hydrogel groups (Fig. 2E).

By conducting compression tests to determine the Young's modulus of various groups of hydrogels. The stress–strain curves for each group of hydrogels are shown in Fig. 2 F, Alg

hydrogel exhibited the highest Young's modulus, with a value of 1.7 kPa (Fig. 2G). In contrast, the Young's modulus of Alg-Mg hydrogel was slightly lower at 1.2 kPa, while the Young's modulus of Alg-Mg/SF hydrogel and Alg/SF hydrogel were measured at 1.1 kPa and 0.9 kPa, respectively.
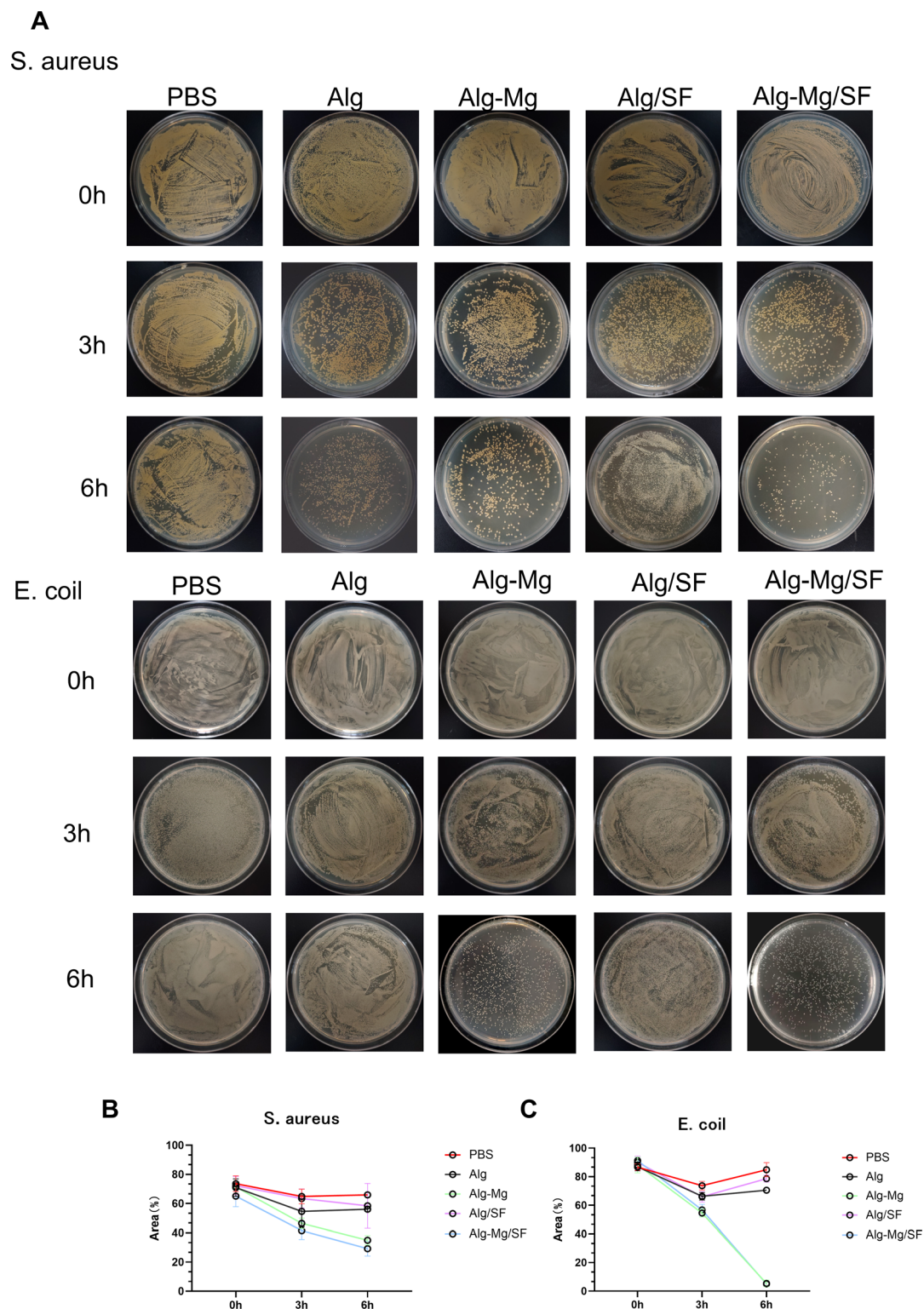
Fig. 3 Antibacterial activity of Alg–Mg/SF hydrogel. (A) Survival *E. coli* clones and *S. aureus* clones on agar plate after contacting with hydrogels. (B) Surface antibacterial activity of hydrogels for *E. coli*. (C) Surface antibacterial activity of hydrogels for *S. aureus*.

In the strain sweep oscillatory experiments (Fig. 2H), all hydrogels consistently exhibited higher G' than G'' at 1% strain, maintaining stability. Beyond the linear region, G' starts to decline, indicating the onset of yield stress and plastic deformation in the system. Hydrogel with higher yield stress and G' values show greater resistance to deformation. It is noteworthy that Alg-SF and Alg-Mg/SF hydrogels did not reach their yield points even at 100% strain. At 10% strain in the Alg and Alg-Mg hydrogel groups, the crossover point of G' and G'' suggests that Alg and Alg-Mg hydrogels have relatively lower deformation resistance compared to the other groups.

In vitro antibacterial efficiency

Gram-positive *Staphylococcus aureus* and Gram-negative *Escherichia coli* are two common pathogenic bacteria. Therefore, we evaluated the antibacterial performance of various hydrogel groups against these two strains. The bacteria were directly in contact with the hydrogels for 3 hours and 6 hours at
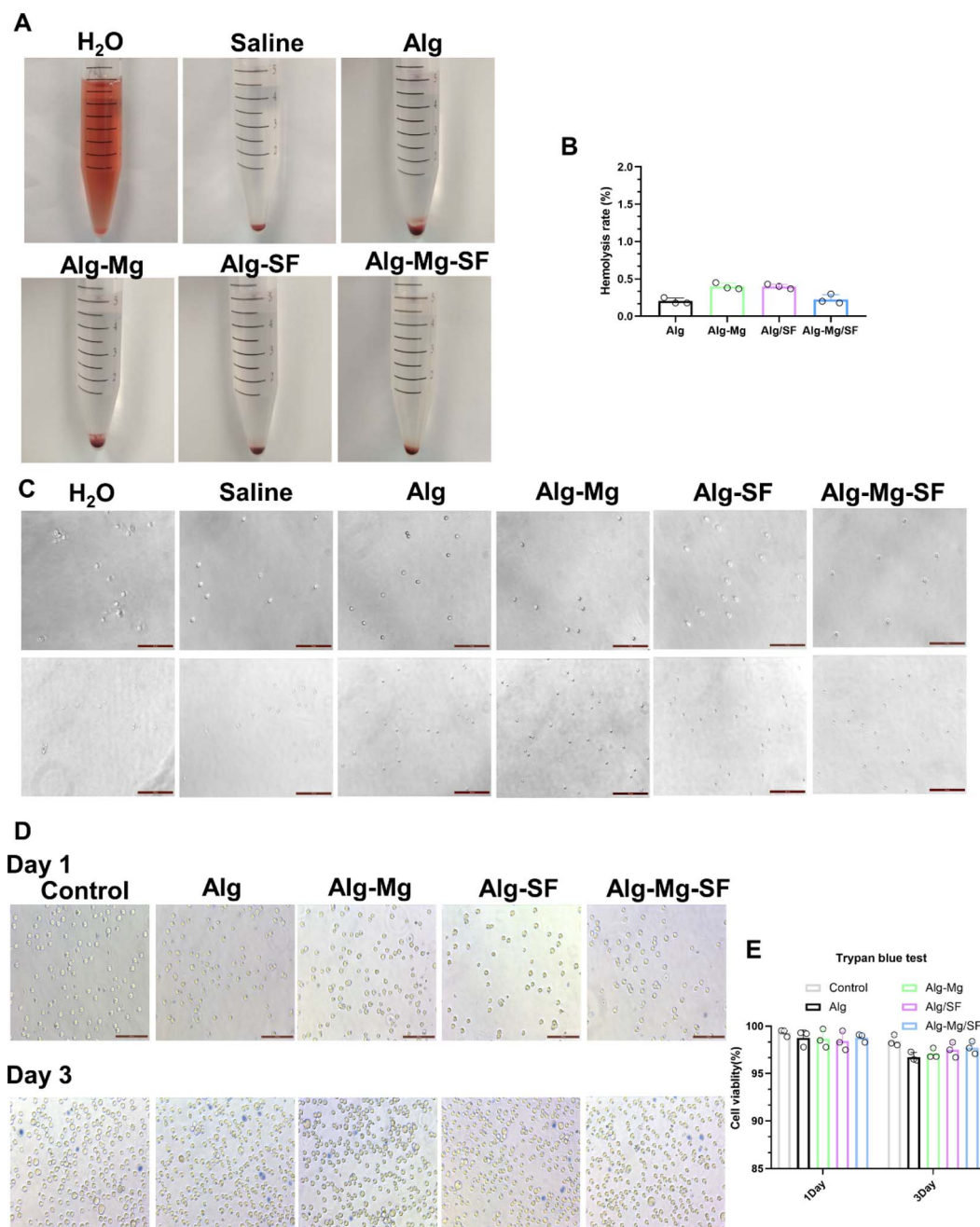

Fig. 4 Excellent biocompatibility of Alg-Mg/SF hydrogel. (A) Photograph of red blood cells co-incubated with negative control, Saline, and Alg-Mg/SF hydrogels for 1 h. (B) Hemolysis ratio of different groups. (C) Typical hemolysis images of different treatment groups; scale bars, 50 μm in the upper row and 100 μm in the lower row, respectively. (D) Bright-field images of L929 cells co-cultured with Alg-Mg/SF hydrogel for 1 day and 3 days under toluidine blue staining; scale bars = 100 μm. (E) The survival rates after co-cultivation with L929 cells differ among various hydrogel groups.

37 °C. As shown in Fig. 3A, after 3 hours of direct contact with various hydrogels, all hydrogel groups exhibited inhibitory activity against both bacterial strains. However, under the conditions of direct contact for 6 hours, Alg-Mg/SF hydrogel showed the highest inhibition rate against *Staphylococcus aureus* (70%), followed by the Alg-Mg hydrogel group with magnesium ions (60%). The inhibition rates for Alg and Alg-Mg hydrogel groups without magnesium ions were only 35%. For *Escherichia coli*, the inhibition rates for Alg and Alg/SF hydrogel groups were only around 20%, while hydrogels containing sustained-release magnesium ions, Alg-Mg, and Alg-Mg/SF, achieved antibacterial rates exceeding 95% (Fig. 3B and C). These results clearly indicate that Alg-Mg and Alg-Mg/SF hydrogels with sustained-release magnesium ions demonstrate continuous and efficient antibacterial capabilities.

Biocompatibility of hydrogels

The hemocompatibility of the alginate-based hydrogel variants was quantified utilizing a standardized hemolysis assay. Observations of erythrocyte morphology under the microscope revealed that red blood cells maintained their structural integrity across all samples, with no evident hemolysis when contacted with the hydrogels (Fig. 4A and C). Statistical analysis of the hemolysis assay revealed minimal red blood cell lysis by the Alg, Alg-Mg, Alg-Mg/SF, and Alg-SF hydrogels, with hemolysis percentages comfortably residing within acceptable range of biosafety (Fig. 4B). This low level of hemolysis corroborates the

non-disruptive interaction between the hydrogels and erythrocytes, signifying the hydrogels' suitability as biomaterials in antimicrobial applications.

Biocompatibility stands as a fundamental criterion ensuring the safe application of medical devices. To assess the cell biocompatibility of the hydrogels, a CCK8 assay was performed using L929 fibroblast cells. As depicted in Fig. S1,† all groups of hydrogels exhibited cell viabilities exceeding 85%, thus affirming the non-toxic nature of these materials.

Fibroblasts is One of the most crucial cellular components in the dermis of the skin. Therefore, trypan blue test was conducted to assess the cell viability under the contact of hydrogels with L929 cells. In this experiment, viable cells remain unstained, while dead cells appear light blue. As shown in Fig. 4D, the results indicate that after co-cultivation with various hydrogel groups, over 95% of L929 cells remain unstained, maintaining their normal morphology and luster (Fig. 4E). Only a small number of cells appear light blue and swollen, losing their luster. This suggests that the contact between hydrogels and L929 cells is safe for the majority of cells, preserving their normal state. Only a small fraction of cells appears light blue, swollen, and lacking luster.

Immunological analysis of Alg-Mg/SF hydrogel for early induction of macrophage polarization

Anti-inflammatory properties are pivotal in antimicrobial materials, as they significantly reduce infection-related
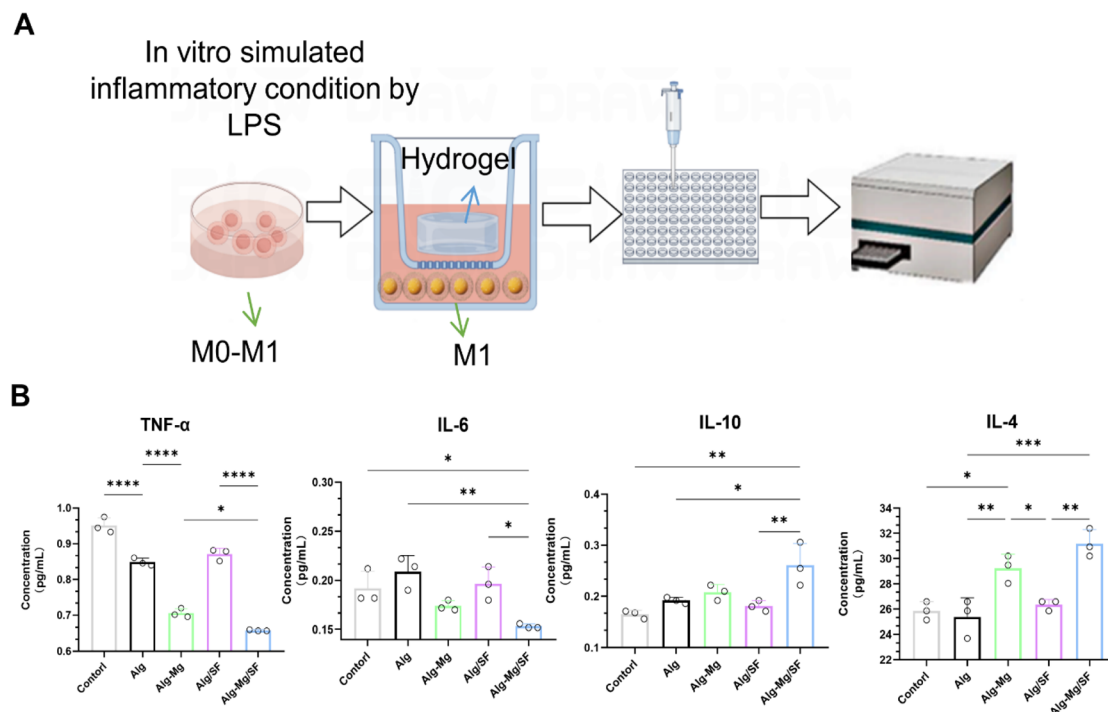

Fig. 5 The Alg-Mg/SF hydrogel promotes the secretion of anti-inflammatory factors by macro. (A) Lipopolysaccharide stimulation can induce the transformation of macrophages from M0 to the M1 phenotype. Following co-cultivation with different hydrogel groups, the concentrations of pro-inflammatory and anti-inflammatory factors secreted by macrophages were assessed using Elisa. (B) After 3 days of co-cultivation, the concentrations of pro-inflammatory factors TNF-α and IL-6, as well as anti-inflammatory factors IL-10 and IL-4 ($n = 3$); *$p < 0.05$, **$p < 0.01$, ***$p < 0.001$, ****$p < 0.0001$.

inflammation, thereby enhancing wound healing. Raw264.7 cells were induced to transform into M1-type macrophages through lipopolysaccharide stimulation, followed by co-cultivation with hydrogels from different groups for 3 days (Fig. 5A).

Quantitative ELISA assays were utilized to measure the concentrations of cytokines IL-6, TNF-α, IL-10, and IL-4. Observations revealed a suppressed expression of the pro-inflammatory cytokines IL-6 and TNF-α in the Alg-SF/Mg and Alg-Mg hydrogel groups. Conversely, the levels of the anti-inflammatory cytokines IL-10 and IL-4 were elevated in these groups when compared to the Alg and Alg/SF controls. Notably, the Alg-Mg/SF hydrogel composition presented the most significant elevation in IL-10 concentration, suggesting an enhanced anti-inflammatory potential (Fig. 5B).

Discussion

Wound infection typically leads to prolonged healing time, implant failure, and can result in other serious complications, even death. The preparation method of hydrogel wound dressings determines their fundamental performance. Due to differences in bond energy, chemically cross-linked hydrogels generally exhibit high strength; however, irreversible damage occurs when covalent bonds are disrupted under external forces. On the other hand, ionically cross-linked hydrogels usually demonstrate weaker mechanical properties. In this study, we prepared Alg-Mg/SF hydrogels with an intertwined network of magnesium ions and silk fibroin protein. The Alg-Mg/SF hydrogel, compared to Alg and Alg-Mg single-network hydrogels, showed higher strain resistance, indicating a more stable hydrogel network. This enhanced strain resistance is attributed to the intertwined network formed by SF-GSH and SF-MA through click chemistry, followed by the formation of a network with sodium alginate. This design not only enhances the mechanical performance of Alg-Mg/SF hydrogel but also facilitates its response to potential complexities in antibacterial experiments, particularly in its application in animal.[27]

The release of metal ions (Ag, Zn, Au, Cu, Mg) to achieve antibacterial effects has gained attention. Metal or metal oxide particles can bind with active enzymes inside bacterial cells, directly attacking DNA, proteins, and other active substances, leading to oxidative stress and eventual bacterial death.[28,29]. However, uncontrolled rapid release of metal ions can lead to accumulation and toxicity. In this study, we modified sodium alginate with bisphosphonates (BPs) using the carbodiimide chemistry method. The Alg-Mg/SF hydrogel, formed by cross-linking with magnesium ions through the coordination bonds of bisphosphonates, exhibited stable release of magnesium ions for up to two weeks, avoiding a cascade release. In anti-bacterial experiments, Alg-Mg/SF and Alg-Mg hydrogels demonstrated excellent contact-active antibacterial activity. The outstanding antibacterial performance is attributed to the controlled release of magnesium ions in the hydrogel, achieving broad-spectrum antibacterial activity. In contrast, Alg and Alg/SF hydrogels, lacking magnesium ions, showed limited antibacterial capabilities.

Developing a hydrogel with both excellent cell affinity and outstanding antibacterial capabilities is a challenging task. The unique properties of sodium alginate are particularly noteworthy as a natural polysaccharide with excellent biocompatibility.[30] In our previous studies, Alg-Mg/SF hydrogel showed outstanding biocompatibility in the field of neural tissue engineering. Importantly, after 3 days of co-cultivation with various hydrogel groups in this study, L929 cells exhibited a survival rate as high as 95%. All hydrogel groups also demonstrated good blood compatibility. This clearly indicates that Alg-Mg/SF hydrogel not only maintains its excellent antibacterial ability but also ensures superior biocompatibility with cells.

In the field of wound healing and repair, the design of biomaterials should not only focus on excellent antimicrobial performance but also pay attention to the regulation of inflammatory responses during wound healing. Excessive inflammation responses may bring additional suffering to patients. Magnesium ions have a significant impact on the regulation of immune cells, prompting the immune system to respond to external stimuli in a more balanced and harmonious manner. This balance helps avoid excessive inflammatory responses, reducing the risk of tissue damage. Similarly, the Alg-Mg/SF hydrogel designed in our study can regulate macrophages to secrete more anti-inflammatory factors IL-10 and IL-4. This suggests that Alg-Mg/SF hydrogel may help balance the inflammation process at the wound site and contribute to maintaining a stable wound microenvironment, ultimately alleviating inflammation-induced tissue damage.

Conclusion

In summary, we have presented an antibacterial intertwined Alg-Mg/SF hydrogel, achieving a synergistic combination of effective antibacterial capability and outstanding cell affinity. The metal coordination between bisphosphonates and magnesium ions in the hydrogel imparts long-lasting and effective antibacterial properties. This not only avoids many issues associated with antibiotic use, including high costs, short half-life, bacterial resistance, and burst release but also provides a new solution for balancing antibiotics. Moreover, the release of magnesium ions can regulate macrophages to secrete abundant IL-10 and TGF-β, inhibiting inflammation. This is anticipated to contribute to tissue repair, remodeling, angiogenesis, and maintaining homeostasis. In conclusion, this study introduces a novel strategy for forming active antibacterial hydrogels, offering promising support for future medical treatments and tissue engineering research.

Author contributions

Y. Y., Q. X. and Y. Z. conceived and designed the experiments. C. D., B. W., M. C., Y. G., M. Z. and W. L. performed the experiments. Y. S. and M. Z. analyzed the data. G. L., Q. X. and Y. Z. contributed reagents/materials/analysis tools. Y. Z. and Y. G. wrote the manuscript. All authors read and approved the final manuscript.

Conflicts of interest

The authors declare that they have no conflict of interest.

Acknowledgements

References

1 Y. Liang, Y. Liang, H. Zhang and B. Guo, *Asian J. Pharm. Sci.*, 2022, **17**, 353–384.

2 M. Chen, J. Tian, Y. Liu, H. Cao, R. Li, J. Wang, J. Wu and Q. Zhang, *Chem. Eng. J.*, 2019, **373**, 413–424.

3 B. Jia, G. Li, E. Cao, J. Luo, X. Zhao and H. Huang, *Mater. Today Bio*, 2023, **16**(19), 100582.

4 Y. Zhong, H. Xiao, F. Seidi and Y. Jin, *Biomacromolecules*, 2020, **21**, 2983–3006.

5 E. R. Ghomi, S. Khalili, S. N. Khorasani, R. E. Neisiany and S. Ramakrishna, *J. Appl. Polym. Sci.*, 2019, **136**(27), DOI: **10.1002/app.47738**.

6 S. Li, S. Dong, W. Xu, S. Tu, L. Yan, C. Zhao, J. Ding and X. Chen, *Adv. Sci.*, 2018, **5**(5), DOI: **10.1002/advs.201700527**.

7 G. D. Mogosanu and A. M. Grumezescu, *Int. J. Pharm.*, 2014, **463**, 127–136.

8 M. H. Norahan, S. C. Pedroza-Gonz, M. G. Sanchez-Salazar, M. M. Alvarez and G. T. de Santiago, *Bioact. Mater.*, 2023, **24**, 197–235.

9 Y. Lu, C. Liu, C. Mei, J. Sun, J. Lee, Q. Wu, M. A. Hubbe and M.-C. Li, *Coord. Chem. Rev.*, 2021, **9**(41), DOI: **10.1016/j.ccr.2022.214496**.

10 Z. Shen, C. Zhang, T. Wang and J. Xu, *Polymers*, 2000, **15**(9), DOI: **10.3390/polym15092000**.

11 Z. Cao, Y. Luo, Z. Li, L. Tan, X. Liu, C. Li, Y. Zheng, Z. Cui, K. W. K. Yeung, Y. Liang, S. Zhu and S. Wu, *Macromol. Biosci.*, 2020, **21**(1), DOI: **10.1002/mabi.202000252**.

12 J.-Y. Ji, D.-Y. Ren and Y.-Z. Weng, *Int. J. Nanomed.*, 2022, **17**, 3163–3176.

13 N. Asadi, H. Pazoki-Toroudi, A. R. Del Bakhshayesh, A. Akbarzadeh, S. Davaran and N. Annabi, *Int. J. Biol. Macromol.*, 2021, **170**, 728–750.

14 P. Makvandi, C. Wang, E. N. Zare, A. Borzacchiello, L. Niu and F. R. Tay, *Adv. Funct. Mater.*, 2020, **30**(22), DOI: **10.1002/adfm.201910021**.

15 J. Liu, W. Jiang, Q. Xu and Y. Zheng, *Gels*, 2022, **8**(8), DOI: **10.3390/gels8080503**.

16 Q. He, T. Tong, C. Yu and Q. Wang, *Mar. Drugs*, 2023, **21**(1), DOI: **10.3390/md21010014**.

17 B. A. Aderibigbe and B. Buyana, *Pharmaceutics*, 2018, **10**(2), DOI: **10.3390/pharmaceutics10020042**.

18 W. Peng, D. Li, K. Dai, Y. Wang, P. Song, H. Li, P. Tang, Z. Zhang, Z. Li, Y. Zhou and C. Zhou, *Int. J. Biol. Macromol.*, 2022, **208**, 400–408.

19 K. Varaprasad, T. Jayaramudu, V. Kanikireddy, C. Toro and E. R. Sadiku, *Carbohydr. Polym.*, 2020, **236**, 116025.

20 M. C. Catoira, L. Fusaro, D. Di Francesco, M. Ramella and F. Boccafoschi, *J. Mater. Sci.: Mater. Med.*, 2019, **30**(10), DOI: **10.1007/s10856-019-6318-7**.

21 A. Manzoor, A. H. Dar, V. K. Pandey, R. Shams, S. Khan, P. S. Panesar, J. F. Kennedy, U. Fayaz and S. A. Khan, *Int. J. Biol. Macromol.*, 2022, **213**, 987–1006.

22 M. Shen, F. Forghani, X. Kong, D. Liu, X. Ye, S. Chen and T. Ding, *Compr. Rev. Food Sci. Food Saf.*, 2020, **19**, 1397–1419.

23 E. Zhang, X. Zhao, J. Hu, R. Wang, S. Fu and G. Qin, *Bioact. Mater.*, 2021, **6**, 2569–2612.

24 D. Franco, G. Calabrese, S. P. P. Guglielmino and S. Conoci, *Microorganisms*, 2022, **10**(9), DOI: **10.3390/microorganisms10091778**.

25 N. Sezer, Z. Evis, S. M. Kayhan, A. Tahmasebifar and M. Koc, *J. Magnesium Alloys*, 2018, **6**, 23–43.

26 Y. Gao, Y. Wang, J. Zhang, M. Zhang, C. Dai, Y. Zhang, L. Zhang, L. Bian, Y. Yang, K. Zhang and Y. Zhao, *Bioact. Mater.*, 2024, **33**, 100–113.

27 D. Gan, T. Xu, W. Xing, X. Ge, L. Fang, K. Wang, F. Ren and X. Lu, *Adv. Funct. Mater.*, 2019, **29**(1), DOI: **10.1002/adfm.201805964**.

28 Y. Liu, W. Ma, W. Liu, C. Li, Y. Liu, X. Jiang and Z. Tang, *J. Mater. Chem.*, 2011, **21**, 19214–19218.

29 Y. Liu, F. Li, Z. Guo, Y. Xiao, Y. Zhang, X. Sun, T. Zhe, Y. Cao, L. Wang, Q. Lu and J. Wang, *Chem. Eng. J.*, 2020, **382**, 122990.

30 W.-C. Huang, R. Ying, W. Wang, Y. Guo, Y. He, X. Mo, C. Xue and X. Mao, *Adv. Funct. Mater.*, 2020, **30**(21), DOI: **10.1002/adfm.202000644**.